European Journal of Protistology 94 (2024) 126075

Contents lists available at ScienceDirect

European Journal of Protistology

journal homepage: www.elsevier.com/locate/ejop

Homo- and hetero-oligomeric protein–protein associations explain autocrine and heterologous pheromone-cell interactions in *Euplotes*

Claudio Alimenti [a], Bill Pedrini [b], Pierangelo Luporini [a], Yaohan Jiang [a,c], Adriana Vallesi [a,*]

[a] School of Biosciences and Veterinary Medicine, University of Camerino, Camerino, MC, Italy
[b] Paul Scherrer Institute, 5232 Villigen PSI, Switzerland
[c] Institute of Evolution & Marine Biodiversity, Ocean University of China, Qingdao 266003, China

ARTICLE INFO

Keywords:
Self/not-self recognition
Water-borne pheromones
Protein crystal structures
Protein oligomerization
Euplotes mating

ABSTRACT

In *Euplotes*, protein pheromones regulate cell reproduction and mating by binding cells in autocrine or heterologous fashion, respectively. Pheromone binding sites (receptors) are identified with membrane-bound pheromone isoforms determined by the same genes specifying the soluble forms, establishing a structural equivalence in each cell type between the two twin proteins. Based on this equivalence, autocrine and heterologous pheromone/receptor interactions were investigated analyzing how native molecules of pheromones E*r*-1 and E*r*-13, distinctive of mating compatible *E. raikovi* cell types, associate into crystals. E*r*-1 and E*r*-13 crystals are equally formed by molecules that associate cooperatively into oligomeric chains rigorously taking a mutually opposite orientation, and each burying two interfaces. A minor interface is pheromone-specific, while a major one is common in E*r*-1 and E*r*-13 crystals. A close structural inspection of this interface suggests that it may be used by E*r*-1 and E*r*-13 to associate into heterodimers, yet inapt to further associate into higher complexes. Pheromone-molecule homo-oligomerization into chains accounts for clustering and internalization of autocrine pheromone/receptor complexes in growing cells, while the heterodimer unsuitability to oligomerize may explain why heterologous pheromone/receptor complexes fail clustering and internalization. Remaining on the cell surface, they are credited with a key role in cell–cell mating adhesion.

1. Background

Among evolutionarily more successful and experimentally more promising ciliates, *Euplotes* calls for a privileged position. It is represented by nearly one hundred morphospecies that are regular components of any food web and colonizers of the most disparate habitats including abyssal depths (Živaljić et al., 2020), hypersaline lagoons (Fotedar et al., 2016) and high-latitude freezing waters (Di Giuseppe et al., 2011; 2013; 2015). The extraordinary genetic variation underlying this evolutionary success is largely explained by the adoption of a strongly outbreeding lifestyle, which results from cell-cell mating interactions and inter-population gene flow controlled through high-multiple systems of mating-types (Nobili et al., 1978). These systems act via species-specific families of diffusible signal proteins, nowadays commonly reported as pheromones, each specified by one of a series of multiple alleles (usually designated *mat-1*, *mat-2*, *mat-3* and so forth) that are inherited in Mendelian fashion at the *mat*-locus of the chromosomic micronuclear genome (Heckmann, 1963; Nobili et al., 1978), and expressed as gene-size DNA molecules in the sub-chromosomic macronuclear genome (Ricci et al., 2019; Vallesi et al., 2012).

The most apparent pheromone activity is sexual, manifested as heterologous (not-self) induction of cell–cell unions in mating pairs. It was originally discovered in *E. patella* by Kimball (1942), who observed that genetically identical cells were promptly induced to unite in mating pairs following suspension with supernatant preparations from cultures of genetically different cell types. This sexual activity has for long time been regarded as the unique pheromone activity, receiving experimental support (Miyake, 1981) particularly from the chemical characterization of two structurally unrelated mating active molecules, a glycoprotein and a tryptophan derivative (named "gamones"), isolated from cultures of *Blepharisma japonicum* and assigned to represent two functionally distinct cell types (improperly defined as 'sexually complementary', lacking any information on their genetic determinants and native *Blepharisma* cells regularly practicing self-mating). The late arrival of *E. raikovi* pheromones onto the scene has eventually provided evidence that the pheromone sexual activity is not unique, but rather likely

* Corresponding author.
E-mail address: adriana.vallesi@unicam.it (A. Vallesi).

https://doi.org/10.1016/j.ejop.2024.126075

Available online 16 March 2024
0932-4739/© 2024 The Authors. Published by Elsevier GmbH. This is an open access article under the CC BY license (http://creativecommons.org/licenses/by/4.0/).

secondarily acquired in the course of evolution with respect to the less apparent, yet primary autocrine (autologous) activity aimed at promoting the mitotic reproduction (growth) of the same cells from which pheromones are secreted (Vallesi et al., 1995).

This double biological activity is made possible by the close relationships of pheromone structural homology, which permits members of each species-specific pheromone family to bind target cells in mutual competition (Ortenzi and Luporini, 1995; Ortenzi et al., 1990). As shown by NMR spectroscopy of native protein preparations from *E. raikovi* (Brown et al., 1993; Zahn et al., 2001), *E. nobilii* (Pedrini et al., 2007; Placzek et al., 2007) and *E. petzi* (Pedrini et al., 2017), regardless of variations in amino acid sequences, conspecific pheromones closely mimic one another in their molecular folding basically represented by an up-down-up three-helix bundle stabilized by a conserved pattern of densely spaced disulfide bridges (Alimenti et al., 2009; Luginbühl et al., 1994; Luporini et al., 2016).

In *E. raikovi*, the pheromone binding sites on target cells have been identified with longer insoluble pheromone isoforms represented by single-pass transmembrane type-II proteins, having the C-terminus exposed on the extracellular side and the N-terminus on the cytoplasmic side (Miceli et al., 1992; Ortenzi et al., 2000). These pheromone isoforms, henceforth regarded as pheromone receptors, are synthesized through a mechanism of intron splicing by the same macronuclear pheromone genes which encode the soluble pheromone molecules in the form of immature cytoplasmic precursors (pre-pro-pheromones) (Miceli et al., 1992; Ricci et al., 2019, 2021). As a consequence of this common genetic determination, the pheromone receptors of each cell type turn out to repeat the same pre-pro-pheromone sequence at the level of their *trans*-membrane and extracellular ligand-binding domains, and to show a new sequence (including potential phosphorylation sites) at the level of the cytoplasmic domain (Fig. 1).

This structural context, combined with observations from mass spectrometry analysis that native homo- and possibly oligomeric aggregates (with the subunits associated by noncovalent forces) are

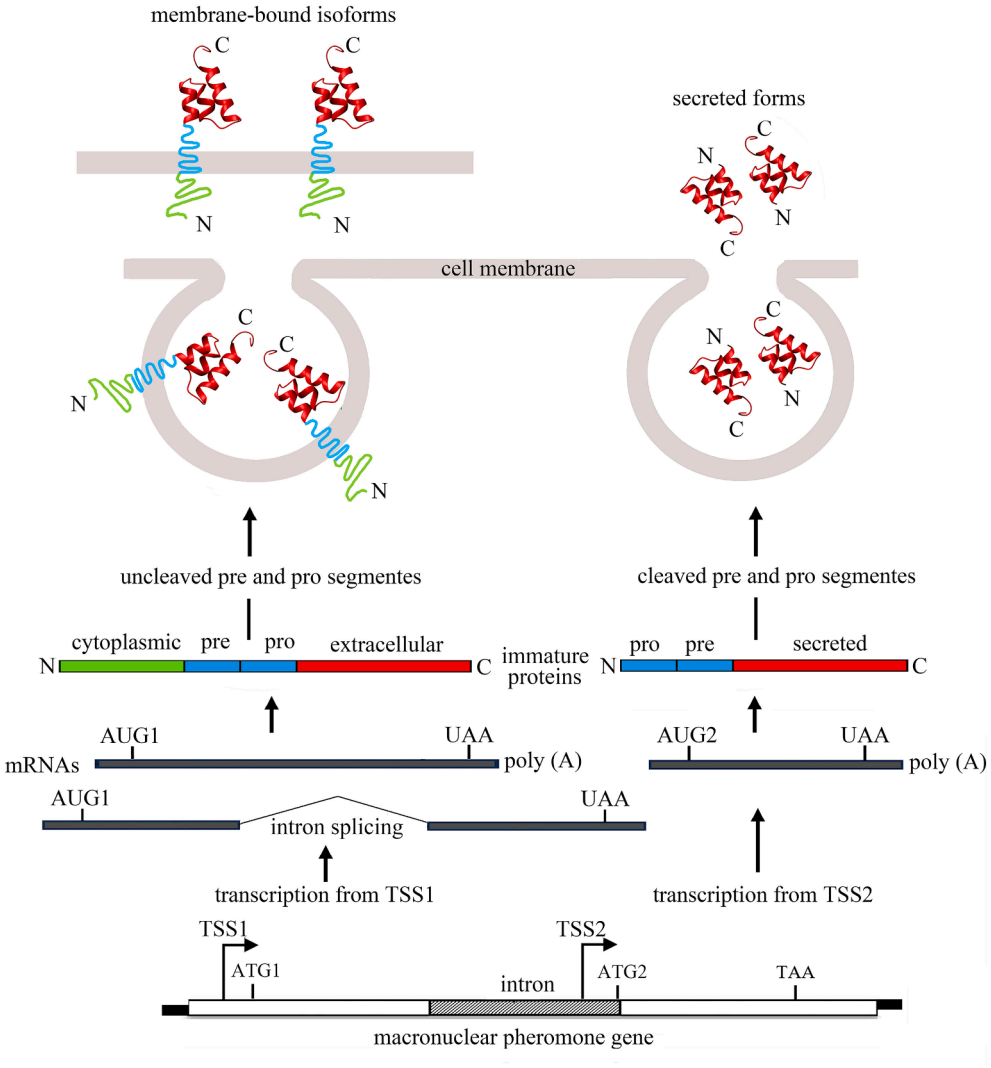

Fig. 1. Schematic representation of the intron-splicing mechanism that in *E. raikovi* macronuclear pheromone genes results in the synthesis of soluble pheromone molecules and longer membrane-bound pheromone isoforms. In the pheromone structure: TSS1 and TSS2, positions of the two transcription start sites; ATG1, ATG2 and TAA, positions of the translation-start and stop codons; dashed box, intron sequence; filled boxes, telomeric ends. Two distinct mRNA sequences are synthesized. The sequence starting from TSS2 encodes a cytoplasmic pheromone precursor (pre-pro-pheromone), subject to enzymatic cleavages that remove the pre and pro segments and release the soluble pheromone form. The sequence starting from TSS1 involves the removal of the intron sequence and encodes a longer pre-pro-pheromone precursor, which avoids cleavages and remains anchored to the cell membrane. It includes an extracellular C-terminal domain formed by the pro-pheromone sequence, a transmembrane domain formed by the pre (signal-peptide) sequence, and a cytoplasmic N-terminal domain formed by a new sequence. The equivalence in structure between soluble and membrane-bound pheromone molecules is highlighted by identical colors. N and C, amino and carboxyl termini, respectively. Based on Ricci et al. (2019).

commonly formed by *E. raikovi* pheromones (Bradshaw et al., 1990), provided a good reason to inquire into the pheromone/receptor interactions on the cell surface by studying how native water-borne pheromone molecules associate into crystals (Weiss et al., 1995). This study has for long time remained confined uniquely to crystals raised from preparations of the 40-amino acid pheromone E*r*-1 distinctive of type-I cells. It provided evidence for a cooperative model of protein–-protein association in which E*r*-1 molecules tightly clasp into linear chains by simultaneously burying two surfaces and rigorously taking mutually opposite orientations as expected for pheromone and receptor molecules interacting on the cell surface (Weiss et al., 1995).

Anew E*r*-1 crystals were eventually raised along with novel crystals of a second pheromone, dubbed E*r*-13 and secreted from type-XIII cells that are strongly mating reactive with type-I cells (Pedrini et al., 2022). A comparative analysis between the two pheromone crystal structures has, in the first place, fully validated the cooperative model of protein–protein association. In addition, it suggests a parsimonious explanation for the formation and the different destiny of the pheromone/receptor complexes that growing and mating cells form of autocrine or heterologous type, respectively, on their surface, and identifies helix-3 (longer and structurally more regular than helices 1 and 2) as the central element of the pheromone/receptor interactions.

2. E*r*-1 and E*r*-13 molecular and crystal structures

A relatively low degree of equivalence (40 %) joins the E*r*-1 and E*r*-13 amino acid sequences extending 40 and 38 residues, respectively (Fig. 2A). The two sequences match in 17 positions, while differing in the others for non-conservative or semi-conservative substitutions. Regardless of these amino acid variations, their up-down-up three-helix folding is to a large extent wholly overlapping and stabilized by the same three-disulfide bond pattern (Fig. 2B). Limiting the calculation of the 'root-mean-square deviation' (RMSD) to the positions of the backbone atoms of residues on the helices 1 and 3, the RMSD value is as little as

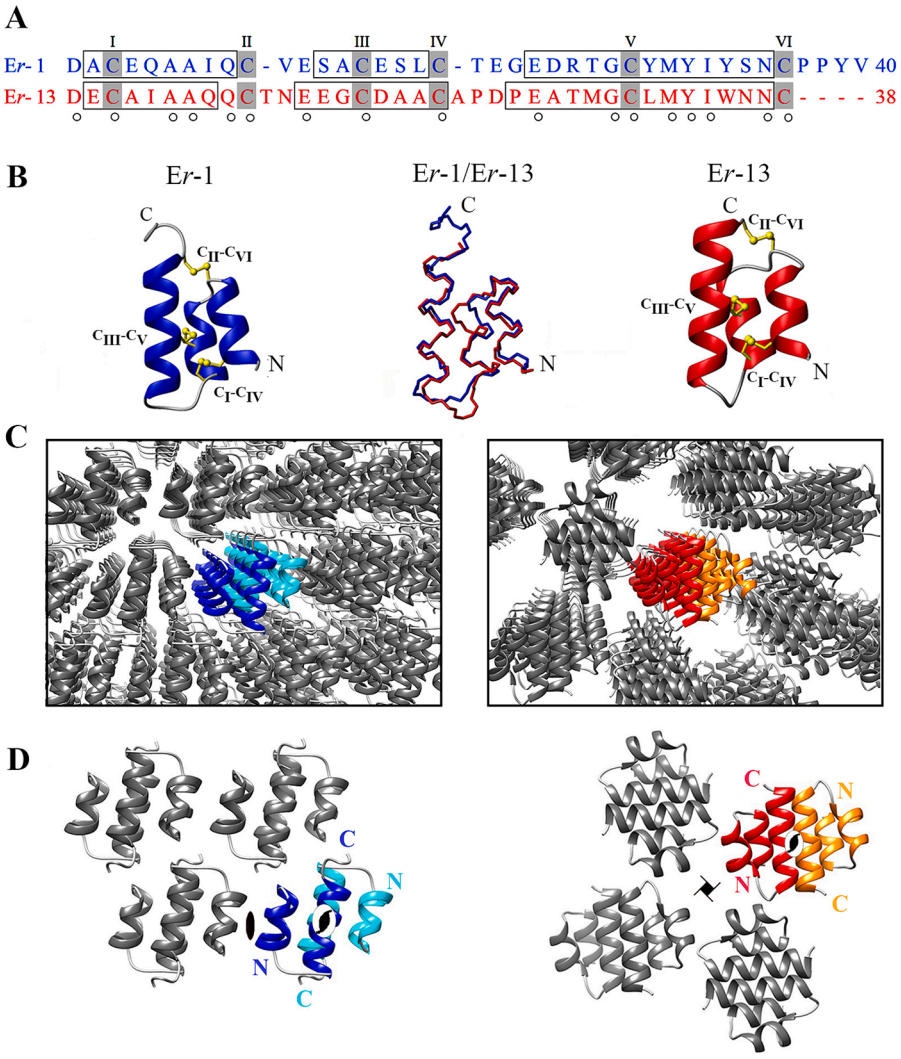

Fig. 2. Amino acid sequences and molecular structures of E*r*-1 and E*r*-13 pheromones. (**A**) Alignment of the E*r*-1 and E*r*-13 amino acid sequences. Boxes enclose residues forming the three helical structures. Cys residues are shadowed and numbered progressively with Roman numerals; dots tag conserved residues. (**B**) Ribbon representations of E*r*-1 and E*r*-13 pheromone folding, and superposition between the two molecular backbones. The three disulfide bridges are represented with yellow ball and stick drawings; N and C, amino and carboxyl termini, respectively. (**C**) Perspective views of the packing array of E*r*-1 and E*r*-13 molecules in the crystal. The mutually opposed orientations taken by molecules within the chains are highlighted by different colors: upside and downside orientated E*r*-1 molecules are colored blue and cyan, respectively; upside and downside orientated E*r*-13 molecules are colored red and orange, respectively. (**D**) Orthogonal projections of the E*r*-1 and E*r*-13 crystal chains along the chain propagation direction. The symmetry axes are indicated with standard symbols; N and C, amino and carboxyl termini, respectively. Based on Pedrini et al. (2022).

0.5 Å. Minor structural variations are confined to the length and configuration of the two inter-helix coil segments, and to the design of helix-2 forming an initial 3_{10}-turn in the E*r*-1 protein while taking a regular α-configuration in the E*r*-13 protein.

The E*r*-1 crystallographic structure was originally determined at a resolution of 1.59 Å (Weiss et al., 1995), and soon refined at 1.0 Å (Anderson et al., 1996, 1997), on crystals with a symmetry of space group *C*2, grown by the sitting-drop vapor diffusion method applied to lyophilized protein dissolved in MilliQ water at a concentration of 8.8 mg/ml. It has ultimately been re-determined at an even higher resolution of 0.7 Å, revealing only a few functionally marginal variations, on crystals that have been freshly synthesized and used in a cross seeding procedure to grow E*r*-13 crystals, showing a symmetry of space group $P4_3$ and analyzed at a resolution of 1.36 Å (Pedrini et al., 2022).

E*r*-1 and E*r*-13 crystals are equally formed by molecules that tightly pack into one-dimensional linear chains running parallel with one another along a two-fold screw symmetry rotation axis parallel to the *c* crystallographic direction (Fig. 2C, D). However, their symmetries differ. A two-fold symmetry (intrinsic to a *C*2 space group) applies to E*r*-1 crystals, while a four-fold screw symmetry (intrinsic to a $P4_3$ space group) applies to E*r*-13 crystals. In the former, inter-chain contacts, earlier described as "dimer 1" (Weiss et al., 1995) and burying an area of approximately 330 $Å^2$, are provided by residues on helices 1 and 2 of facing and inversely oriented molecules of two coplanar adjacent chains. In the latter, instead, inter-chain contacts bury an area of approximately 155 $Å^2$ and are provided by residues mostly lying on inter-helix coil segments of molecules from two chains that are rotated by 90° one with respect to the other.

A substantial difference also distinguishes E*r*-1 and E*r*-13 molecules in relation to their intra-chain arrangement and mutual contacts (Fig. 3A). With respect to E*r*-1 molecules, E*r*-13 molecules settle rotated approximately 30° about the helix axis, and this rotation makes only one protein–protein interface fully equivalent in extension and geometry between E*r*-1 and E*r*-13 chains. This conserved and arguably functionally more relevant interface buries matching areas in E*r*-1 and E*r*-13 chains (590 $Å^2$ and 390 $Å^2$, respectively), and similarly involves contacts between the great majority of residues on helix 3 of one molecule (*n*) and residues on helices 1 and 3 of the nearest (inversely oriented) neighbor molecule (*n–1*). On the other hand, a second interface that molecule *n* shares with its next-nearest (similarly oriented) neighbor molecule (*n–2*) turns out to be appreciably extended (approximately 200 $Å^2$) only in E*r*-13 chains in which it involves contacts between residues on helices 2 and 3 of molecule *n* and residues on helix 1 of molecule *n–2*. Burying only a minimal area of 35 $Å^2$ and involving a single water-molecule mediated contact, it practically lacks in E*r*-1 chains, implying a secondary functional relevance.

3. Biological insights

Different behaviors are known from immunocytochemical observations (Vallesi et al., 1995, 2005) to distinguish the pheromone/receptor complexes of autocrine type that appear on the surface of *Euplotes* cells interacting with their self-pheromone, from the complexes of heterologous type that are formed by mating cells interacting with a not-self pheromone. The autocrine complexes undergo clustering and internalization via endocytic vesicles, whereas the heterologous ones oppose clustering and internalization. It has thus been proposed, on the basis of calculations of protein–protein dimerization forces, that their permanence on the cell surface may function in stabilizing the cell–cell union in mating pairs (Weiss et al., 1995).

As illustrated in Figure 4, the comparative analysis between E*r*-1 and E*r*-13 crystals provides substantial information that accounts for this contrasting behavior between autocrine and heterologous pheromone/receptor complexes. The first piece of information directly pertains to the evidence that molecules of structurally distinct pheromones equally assume mutually opposite orientations to oligomerize into chains. This protein–protein oligomerization pattern precisely mirrors the behavior that is expected from soluble pheromone molecules binding to their twin membrane-bound receptor isoforms bearing the C-terminus oriented outside the cell.

The second piece of information instead relates to functionally significant differences and similarities in the structure of the two surfaces that E*r*-1 and E*r*-13 molecules bury in their common major intra-chain association interface (Fig. 5A). The surface spanning helices 2 and 3 in E*r*-1 molecules and only helix 3 in E*r*-13 molecules is characterized by multiple residue substitutions, which make it a substantially molecule-specific surface. Instead, the surface that in both E*r*-1 and E*r*-13 molecules is provided by helices 1 and 3 turns out to be the site of conservation, or semi-conservation of as many as 14 residues over the total of 16 residues exposed therein. Only two Glu and Asp residues that are unique to E*r*-1 molecules are replaced in E*r*-13 molecules with two Ala residues, causing local and functionally marginal increases in the surface hydrophobicity. This large structural conservation of the helix 1/helix 3 surface thus strongly implies that E*r*-1 and E*r*-13 molecules can mutually utilize it to interact with their specific surface, and likewise with their membrane-bound receptor isoforms, in the formation of heterodimeric complexes.

Two types of E*r*-1/E*r*-13 heterodimers can be expected (Fig. 5B), according to whether an E*r*-1/E*r*-1, or an E*r*-13/E*r*-13 homodimer is taken as a structural prototype for replacing (via minimal RMSD value of the distance between equivalent backbone atoms of residues of helices 1 and 3) one of the two homo-dimeric subunits with a heterologous molecule. In the case where the protein–protein association takes place between the conserved surface of one E*r*-13 molecule and the specific surface of one E*r*-1 molecule, the heterodimer would turn out to be more

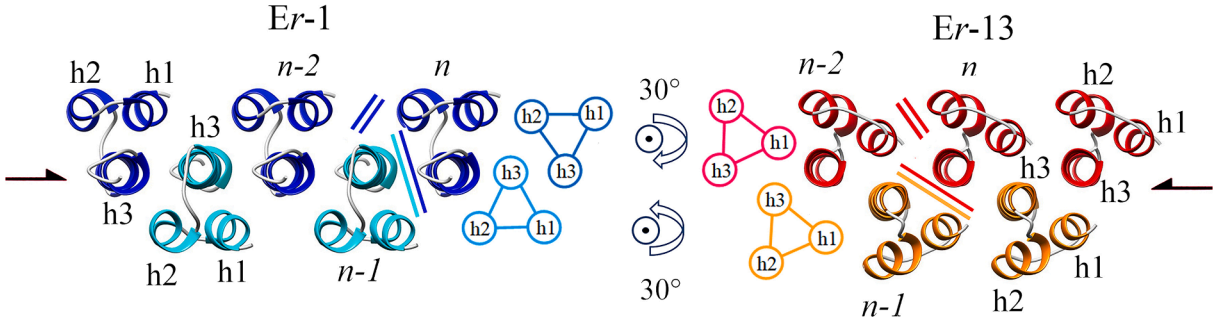

Fig. 3. Top view of E*r*-1 and E*r*-13 crystal chains. Blue and red molecules point the carboxyl terminus towards the observer; instead, cyan and orange molecules point the amino terminus towards the observer. Colored bars indicate the two (one minor and one major) contact interfaces that each molecule (*n*) establishes with the nearest neighbor (*n–1*) and the next-nearest neighbor (*n–2*) molecules. The chain two-fold screw symmetry is indicated with the standard symbol, and the three alpha helices of the E*r*-1 and E*r*-13 molecular folding are marked h1, h2 and h3, respectively. Colored triangles replace ribbon representations to better visualize the rotation of 30° about the helix axis that distinguishes the intra-chain arrangement of E*r*-13 molecules with respect to E*r*-1 molecules. Based on Pedrini et al. (2022).

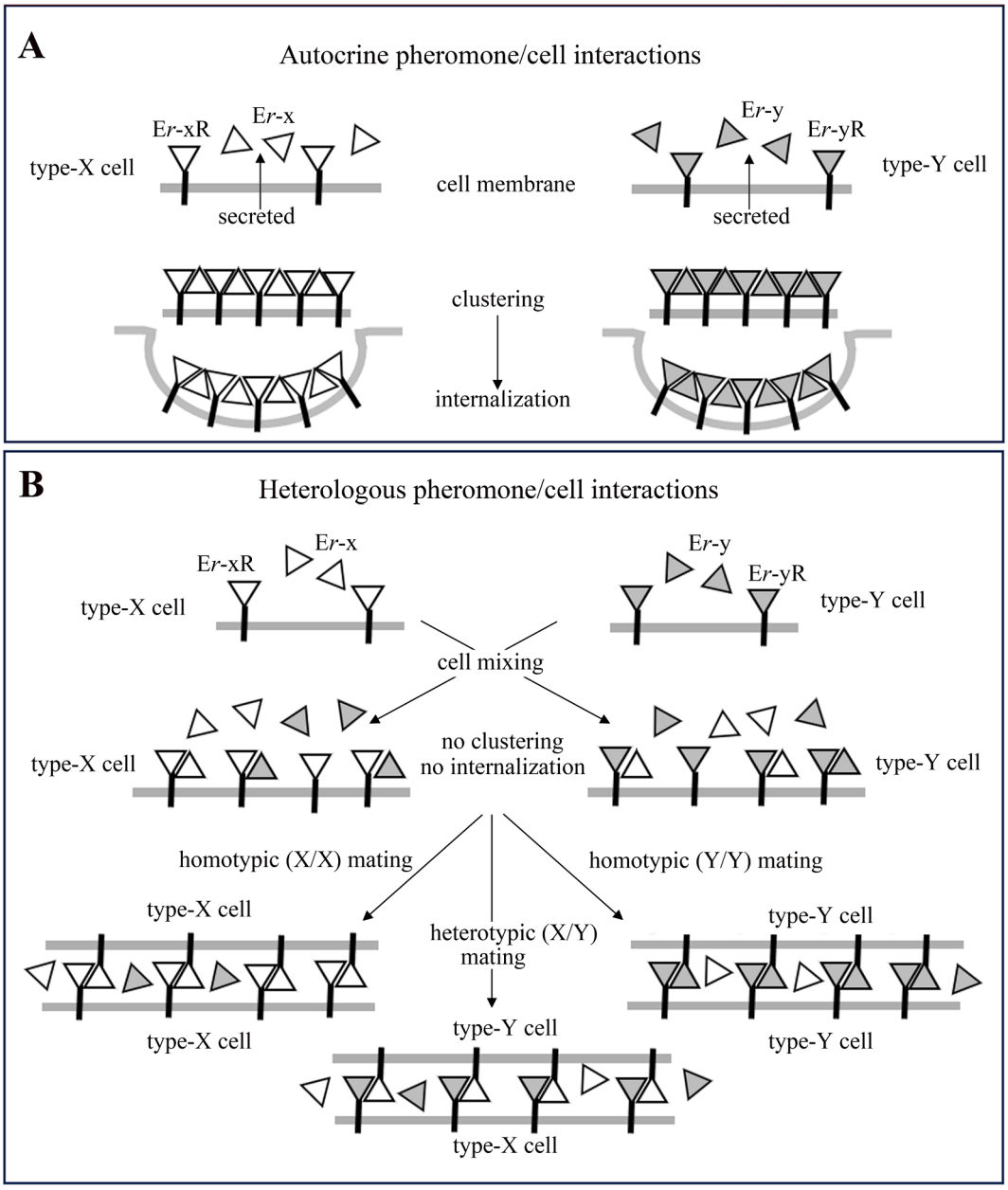

Fig. 4. Schematic representation of the different destinies that in *E. raikovi* (and likely in other *Euplotes* species) distinguish homo- and heterodimeric complexes formed between soluble pheromone molecules and twin membrane-bound isoforms in relation to autocrine (A) and heterologous (B) pheromone/cell interactions. Type-X and type-Y are any two of mutually mating-compatible cell types. Soluble pheromone molecules and membrane-bound receptor isoforms (R) are named E*r*-x and E*r*-xR, respectively, in type-X cells, and E*r*-y and E*r*-yR, respectively, in type-Y cells. It is worth pointing out that *Euplotes*-cell mating interactions regularly generate mating pairs that may equally be of heterotypic (X/Y) or homotypic (X/X, Y/Y) type. Based on immunocytochemical observations from Vallesi et al. (1995), and on protein–protein dimerization forces as originally calculated in E*r*-1 crystals by Weiss et al. (1995) and validated in E*r*-13 crystals by Pedrini et al. (2022).

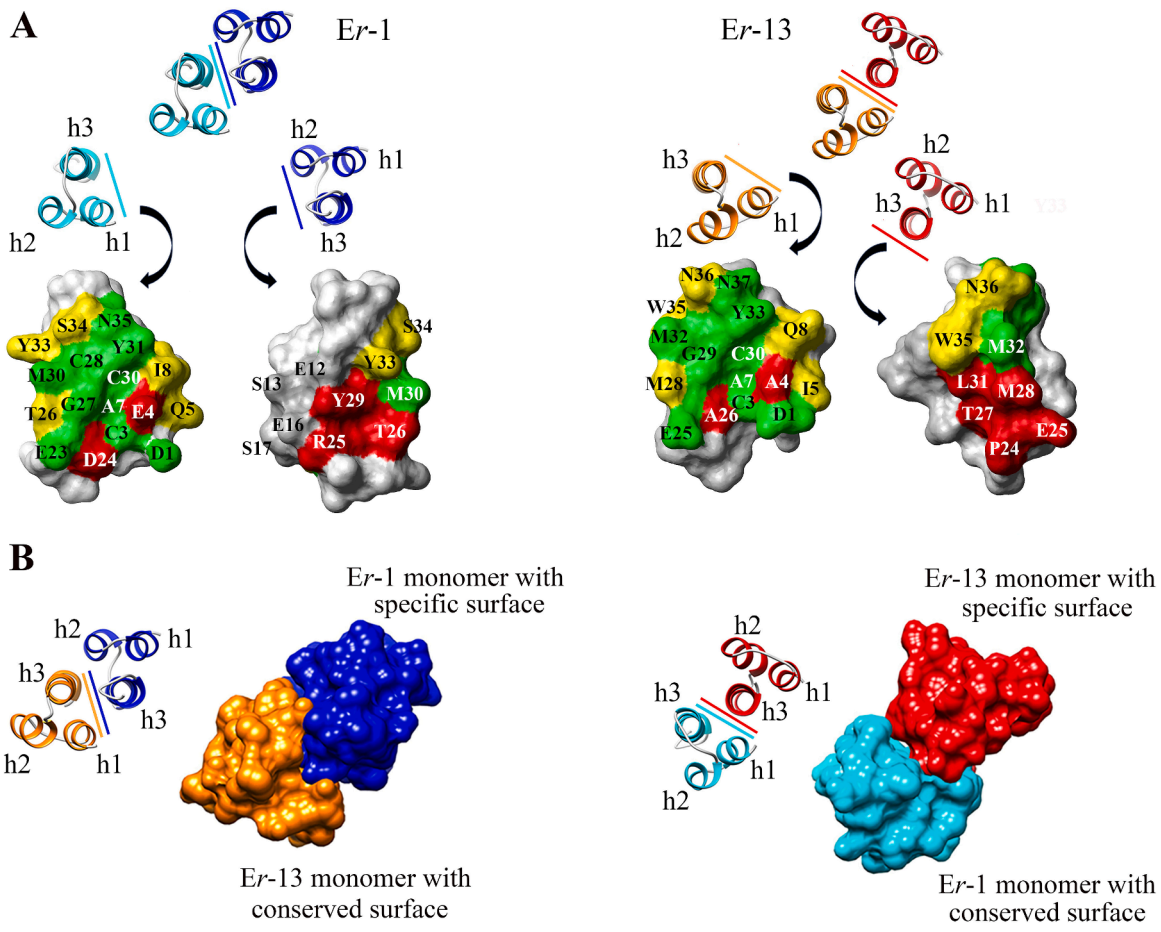

Fig. 5. Heterodimerization between Er-1 and Er-13 molecules. (**A**) Structure of the two surfaces that Er-1 and Er-13 molecules bury in the formation of the major intra-chain interface. Conserved, semi-conserved and not-conserved residues are colored green, yellow and red, respectively. The higher degree of conservation of the surface equally provided by helices 1 and 3 in Er-1 and Er-13 molecules is highlighted by a higher incidence of green; a higher incidence of red instead highlights the higher degree of specificity of the surface provided by helices 2 and 3 in Er-1 molecules and only by helix 3 in Er-13 molecules. The four residues, E12, S13, E16 and S17, on the helix 2/helix 3 surface of Er-1 molecules are not colored, because they lie on helix 2 which is not exposed by Er-13 molecules. (**B**) Diagrammatic representation of the two potential types of heterodimers arising by opposing the conserved surface of one Er-13 molecule to the specific surface of one Er-1 molecule and, vice versa, by opposing the conserved surface of one Er-1 molecule to the specific surface of one Er-13 molecule.

stable, burying a larger interface and relying on the conservation of six out of the seven hydrogen bonds involved in the Er-1/Er-1 homodimerization (Supplementary Table S1). In the alternative case, where the association takes place between the conserved surface of one Er-1 molecule and the specific surface of one Er-13 molecule, the heterodimer would instead turn out to be less stable, burying a smaller and more hydrophobic interface, and involving the disruption of the single hydrogen bond involved in the Er-13/Er-13 homodimerization. This minor stability might thus require reinforcement from supplementary protein–protein associations arising from the utilization of new interfaces. Should these associations take place, their realization in the form of regular linear chains would in any case run into phenomena of clashing and steric collisions, which are the ultimate consequence of the different intra-chain orientation of Er-1 and Er-13 molecules and the most likely reason for frustrating efforts in raising 'hybrid' Er-1/Er-13 crystals (unpublished observations).

Further support as to the functional importance of the structural conservation of the helix 1/helix 3 surface derives from a wider comparison among the molecular structures that have been determined by NMR spectroscopy in other members of the *E. raikovi* pheromone family (Fig. 6). Superimposing the backbones of the two helices for minimal RMSD values provides evidence that the spatial correspondence of most residues forming the helix 1/helix 3 surface is not unique to Er-1 and Er-13 pheromones. Rather, it appears to be a largely shared trait of the pheromone family, and the different extents of structural conservation may be applied to explain variations in the intensity of mating interactions between the respective pheromone-source cell types.

In addition to indications relevant to progress in unravelling the molecular mechanisms that are intrinsic to the autocrine and heterologous pheromone/cell interactions, the Er-1 and Er-13 crystallographic determinations also clearly identify helix-3 as the functionally central element of the pheromone structure. Independently of the variations in their intra-chain arrangement, Er-1 and Er-13 molecules similarly locate their helix 3 right in the middle of the chains in such a way as to charge it with the vast majority of the protein–protein contacts. This functional centrality of helix 3 is reinforced by biological and phylogenetic observations. The former relates to a change in the Er-1 pheromone activity from autocrine to heterologous, which is consequent to cell-ageing phenomena involving the oxidation of the sulfur atom of the Met30 side chain lying well exposed on the helix 3 surface of Er-1 molecules (Alimenti et al., 2012). Native as well as experimental Er-1Met(O) molecules bind their source type-I cells no longer as an autocrine

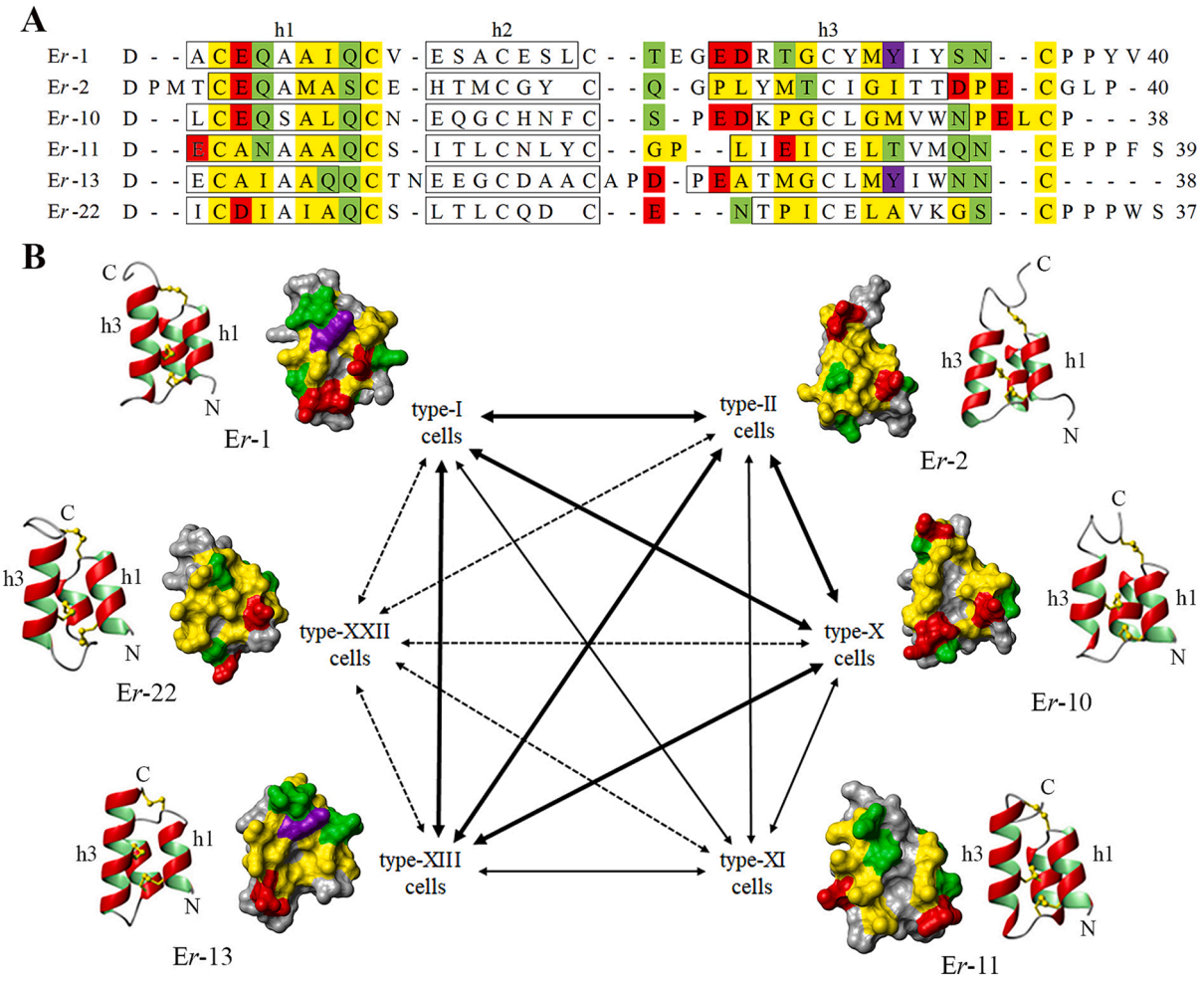

Fig. 6. Amino acid sequences and molecular structures determined in *E. raikovi* pheromones secreted from cell types characterized by varied degrees of mutual mating compatibility. The pheromone Arabic numbering reflects the Roman numbering of the source-cell types. (**A**) Amino acid sequences aligned according to the best positional matching in the corresponding three-dimensional structures (superimposed for minimal backbone RMSD of helices 1 and 3). The residues forming the three helices are boxed and colored on the condition that they expose the side chain on the surface formed by helices 1 and 3. Acid residues (D, E) are in red, aromatic (F, Y, W) in purple, hydrophobic (A, C, G, I, L, M, P, V) in yellow, and polar (N, Q, S, T) in green; no basic residue is contextually involved. (**B**) Visualization of the helix 1/helix 3 molecular surface oriented in front of the observer, as it may better be appreciated by watching the orientation of the molecule ribbon-representations. Strong, moderate and low mating reactions are indicated by thick, thin and dashed double arrows, respectively, which connect the interacting cell types. PDB codes taken as references for the molecular structures: E*r*-1, 6E6O; E*r*-2, 1ERD; E*r*-10, 1ERP; E*r*-11, 1ERY; E*r*-13, 6E6N; E*r*-22, 1HD6.

growth-promoting signal; rather, they bind cells like molecules of a heterologous pheromone inducing the formation of homotypic (self) mating pairs. Considering the double conformation of the Met30 residue that each molecule utilizes in the intra-chain contacts with both the preceding and subsequent nearest neighbors (Pedrini et al., 2022), the cause of the mutated behavior of E*r*-1Met(O) molecules is soundly explained with an enhanced steric hindrance and/or a local modification of the helix 3 surface potential, which makes these molecules no longer amenable to oligomerize (through bilateral contacts) with non-oxidized counterparts.

With regard to phylogenetic observations, an overall comparison of the molecular structures determined from the *E. nobilii*, *E. raikovi* and *E. petzi* pheromone families clearly identifies helix 3 as the most tightly conserved domain in relation to backbone, extension and regular alpha-conformation (Alimenti et al., 2022a; Luporini et al., 2016). Marked reductions in extension and rigid conformation reflecting distinct evolutionary times and varied degrees of environmental cold-adaption (which requires unstructured and flexible regions to face an increased water viscosity) are instead earmarks of helices 1 and 2. They are particularly evident in *E. petzi*, which, in addition to dwelling (like *E. nobilii*) in the freezing polar waters, also takes the most basal position in the *Euplotes* phylogenetic tree (Di Giuseppe et al., 2014; Pedrini et al., 2017). In a functional context, the interspecific helix 3 conservation may also give reason for various observations of mating reactions between sister species such as *E. crassus*, *E. minuta* and *E. vannus* (Nobili et al., 1978), or *E. patella* and *E. octocarinatus* (Kuhlmann and Sato, 1993), as well as of pheromone-mediated mating induction between distantly related *Euplotes* species (Alimenti et al., 2011; 2022b).

CRediT authorship contribution statement

Claudio Alimenti: Investigation, Formal analysis, Conceptualization. **Bill Pedrini:** Validation, Supervision, Investigation, Conceptualization. **Pierangelo Luporini:** Writing – review & editing, Writing – original draft, Supervision, Investigation, Conceptualization. **Yaohan Jiang:** Visualization, Validation, Software. **Adriana Vallesi:** Writing – review & editing, Investigation, Conceptualization.

Declaration of competing interest

The authors declare that they have no known competing financial interests or personal relationships that could have appeared to influence

the work reported in this paper.

Data availability

Data will be made available on request.

Acknowledgments

Financial support was provided by the Italian National Program of Antarctic Research (PNRA) and the Italian Ministry of Research (PRIN project). The authors are grateful to two anonymous reviewers for improving the original version with wise suggestions and constructive criticisms.

Appendix A. Supplementary data

Supplementary data to this article can be found online at https://doi.org/10.1016/j.ejop.2024.126075.

References

Alimenti, C., Vallesi, A., Pedrini, B., Wüthrich, K., Luporini, P., 2009. Molecular cold-adaptation: comparative analysis of two homologous families of psychrophilic and mesophilic signal proteins of the protozoan ciliate, *Euplotes*. IUBMB Life 61, 838–845.

Alimenti, C., Vallesi, A., Federici, S., Di Giuseppe, G., Dini, F., Carratore, V., Luporini, P., 2011. Isolation and structural characterization of two water-borne pheromones from *Euplotes crassus*, a ciliate commonly known to carry membrane-bound pheromones. J. Eukaryot. Microbiol. 58, 234–241.

Alimenti, C., Vallesi, A., Luporini, P., Buonanno, F., Ortenzi, C., 2012. Cell aging-induced methionine oxidation causes an autocrine to paracrine shift of the pheromone activity in the protozoan ciliate *Euplotes raikovi*. Exp. Cell Res. 318, 144–151.

Alimenti, C., Buonanno, F., Di Giuseppe, G., Guella, G., Luporini, P., Ortenzi, C., Vallesi, A., 2022a. Bioactive molecules from ciliates: structure, activity, and applicative potential. J. Eukaryot. Microbiol. 69, e12887.

Alimenti, C., Candelori, A., Jiang, Y., Luporini, P., Vallesi, A., 2022b. Primary structure and coding genes of two pheromones from the Antarctic psychrophilic ciliate *Euplotes focardii*. Microorganisms 10, 1089.

Anderson, D.H., Weiss, M.S., Eisenberg, D., 1996. A challenging case for protein crystal structure determination: the mating pheromone Er-1 from *Euplotes raikovi*. Acta Crystallogr. D Biol. Crystallogr. 52, 469–480.

Anderson, D.H., Weiss, M.S., Eisenberg, D., 1997. Charges, hydrogen bonds, and correlated motions in the 1 Å resolution refined structure of the mating pheromone Er-1 from *Euplotes raikovi*. J. Mol. Biol. 273, 479–500.

Bradshaw, R.A., Raffioni, S., Luporini, P., Chait, B.T., Lee, T., Shively, J., 1990. Amino acid sequence-mass spectrometric analyses of mating pheromones of the ciliate *Euplotes raikovi*. In: Horvath, C., Nikelly, J.G. (Eds.), Analytical Biotechnology. American Chemical Society, Washington, D.C., pp. 153–161

Brown, L.R., Mronga, S., Bradshaw, R.A., Ortenzi, C., Luporini, P., Wüthrich, K., 1993. Nuclear magnetic resonance solution structure of the pheromone Er-10 from the ciliated protozoan *Euplotes raikovi*. J. Mol. Biol. 231, 800–816.

Di Giuseppe, G., Erra, F., Dini, F., Alimenti, C., Vallesi, A., Pedrini, B., Wüthrich, K., Luporini, P., 2011. Antarctic and Arctic populations of the ciliate *Euplotes nobilii* show common pheromone-mediated cell-cell signaling and cross-mating. Proc. Natl. Acad. Sci. USA 108, 3181–3186.

Di Giuseppe, G., Barbieri, M., Vallesi, A., Luporini, P., Dini, F., 2013. Phylogeographical pattern of *Euplotes nobilii*, a protist ciliate with a bipolar biogeographical distribution. Mol. Ecol. 22, 4029–4037.

Di Giuseppe, G., Erra, F., Frontini, F.P., Dini, F., Vallesi, A., Luporini, P., 2014. Improved description of the bipolar ciliate, *Euplotes petzi*, and definition of its basal position in the *Euplotes* phylogenetic tree. Eur. J. Protistol. 50, 402–411.

Di Giuseppe, G., Dini, F., Vallesi, A., Luporini, P., 2015. Genetic relationships in bipolar species of the protist ciliate, *Euplotes*. Hydrobiologia 761, 71–83.

Fotedar, R., Stoeck, T., Filker, S., Fell, J.W., Agatha, S., Al Marri, M., Jiang, J., 2016. Description of the halophile *Euplotes qatarensis* nov. spec. (Ciliophora, Spirotrichea, Euplotida) isolated from the hypersaline Khor Al-Adaid Lagoon in Qatar. J. Eukaryot. Microbiol. 63, 578–590.

Heckmann, K., 1963. Paarungssystem und genabhängige Paarungstypdifferenzierung bei dem hypotrichen Ciliaten *Euplotes vannus* O.F. Müller. Arch. Protistenk. 106, 393–421.

Kimball, R.F., 1942. The nature and inheritance of mating types in *Euplotes patella*. Genetics 27, 269–285.

Kuhlmann, H.W., Sato, K., 1993. Interspecific mating reactions between *Euplotes octocarinatus* and *Euplotes patella* syngen 2. Eur. J. Protistol. 29, 24–31.

Luginbühl, P., Ottiger, M., Mronga, S., Wüthrich, K., 1994. Structure comparison of the pheromones Er-1, Er-10, and Er-2 from *Euplotes raikovi*. Protein Sci. 3, 1537–1546.

Luporini, P., Pedrini, B., Alimenti, C., Vallesi, A., 2016. Revisiting fifty years of research on pheromone signaling in ciliates. Eur. J. Protistol. 55, 26–38.

Miceli, C., La Terza, A., Bradshaw, R.A., Luporini, P., 1992. Identification and structural characterization of a cDNA clone encoding a membrane-bound form of the polypeptide pheromone Er-1 in the ciliate protozoan *Euplotes raikovi*. Proc. Natl. Acad. Sci. USA 89, 1988–1992.

Miyake, A., 1981. Cell interactions by gamones in *Blepharisma*. In: O'Day, D.H., Horgan, P.A. (Eds.), Sexual Interactions in Eukaryotic Microbes. Academic Press, New York, NY, pp. 95–129.

Nobili, R., Luporini, P., Dini, F., 1978. Breeding system, species relationships and evolutionary trends in some species of Euplotidae (Hypotrichida, Ciliata). In: Battaglia, B., Beardmore, J. (Eds.), Marine Organisms. Plenum Press, New York, NY, pp. 591–616.

Ortenzi, C., Alimenti, C., Vallesi, A., Di Pretoro, B., La Terza, A., Luporini, P., 2000. The autocrine mitogenic loop of the ciliate *Euplotes raikovi*: the pheromone membrane-bound forms are the cell binding sites and potential signaling receptors of soluble pheromones. Mol. Biol. Cell 11, 1445–1455.

Ortenzi, C., Luporini, P., 1995. Competition among homologous polypeptide pheromones of the ciliate *Euplotes raikovi* for binding to each other's cell receptors. J. Eukaryot. Microbiol. 42, 242–248.

Ortenzi, C., Miceli, C., Bradshaw, R.A., Luporini, P., 1990. Identification and initial characterization of an autocrine pheromone receptor in the protozoan ciliate *Euplotes raikovi*. J. Cell Biol. 111, 607–614.

Pedrini, B., Placzek, W.J., Koculi, E., Alimenti, C., La Terza, A., Luporini, P., Wüthrich, K., 2007. Cold-adaptation in sea-water-borne signal proteins: sequence and NMR structure of the pheromone E*n*-6 from the Antarctic ciliate *Euplotes nobilii*. J. Mol. Biol. 372, 277–286.

Pedrini, B., Suter-Stahel, T., Vallesi, A., Alimenti, C., Luporini, P., 2017. Molecular structures and coding genes of the water-borne protein pheromones of *Euplotes petzi*, an early diverging polar species of *Euplotes*. J. Eukayot. Microbiol. 64, 164–172.

Pedrini, B., Finke, A.D., Marsh, M., Luporini, P., Vallesi, A., Alimenti, C., 2022. Crystal structure of the pheromone Er-13 from the ciliate *Euplotes raikovi,* with implications for a protein–protein association model in pheromone/receptor interactions. J. Struct. Biol. 214, 107812.

Placzek, W.J., Etezady-Esfarjani, T., Herrmann, T., Pedrini, B., Peti, W., Alimenti, C., Luporini, P., Wüthrich, K., 2007. Cold-adapted signal proteins: NMR structures of pheromones from the Antarctic ciliate *Euplotes nobilii*. IUBMB Life 59, 578–585.

Ricci, F., Candelori, A., Brandi, A., Alimenti, C., Luporini, P., Vallesi, A., 2019. The sub-chromosomic macronuclear pheromone genes of the ciliate *Euplotes raikovi*: comparative structural analysis and insights into the mechanism of expression. J. Eukaryot. Microbiol. 66, 376–384.

Ricci, F., Luporini, P., Alimenti, C., Vallesi, A., 2021. Functional chimeric genes in ciliates: an instructive case from *Euplotes raikovi*. Gene 767, e145186.

Vallesi, A., Giuli, G., Bradshaw, R., Luporini, P., 1995. Autocrine mitogenic activity of pheromones produced by the protozoan ciliate *Euplotes raikovi*. Nature 376, 522–524.

Vallesi, A., Ballarini, P., Di Pretoro, B., Alimenti, C., Miceli, C., Luporini, P., 2005. Autocrine, mitogenic pheromone receptor loop of the ciliate *Euplotes raikovi:* pheromone-induced receptor internalization. Eukaryot. Cell 4, 1221–1227.

Vallesi, A., Alimenti, A., Pedrini, B., Di Giuseppe, G., Dini, F., Wüthrich, K., Luporini, P., 2012. Coding genes and molecular structures of the diffusible signalling proteins (pheromones) of the polar ciliate, *Euplotes nobilii*. Mar. Genomics 8, 9–13.

Weiss, M.S., Anderson, D.H., Raffioni, S., Bradshaw, R.A., Ortenzi, C., Luporini, P., Eisenberg, D., 1995. A cooperative model for receptor recognition and cell adhesion: evidence from the molecular packing in the 1.6-Å crystal structure of the pheromone Er-1 from the ciliated protozoan *Euplotes raikovi*. Proc. Natl. Acad. Sci. USA 92, 10172–10176.

Zahn, R., Damberger, F., Ortenzi, C., Luporini, P., Wüthrich, K., 2001. NMR structure of the *Euplotes raikovi* pheromone Er-23 and identification of its five disulfide bonds. J. Mol. Biol. 313, 923–931.

Živaljić, S., Scherwass, A., Schoenle, A., Hohlfeld, M., Quintela-Alonso, P., Nitsche, F., Arndt, H., 2020. A barotolerant ciliate isolated from the abyssal deep sea of the North Atlantic: *Euplotes dominicanus* sp. n. (Ciliophora, Euplotia). Eur. J. Protistol. 73, e12125664.